INTERNATIONAL JOURNAL OF
NUMERICAL ANALYSIS AND MODELING
Volume 21, Number 6, Pages 910–932

doi: 10.4208/ijnam2024-1036

A FINITE VOLUME METHOD PRESERVING THE INVARIANT REGION PROPERTY FOR THE QUASIMONOTONE REACTION-DIFFUSION SYSTEMS

HUIFANG ZHOU*, YUCHUN SUN, AND FUCHANG HUO

Abstract. We present a finite volume method preserving the invariant region property (IRP) for the reaction-diffusion systems with quasimonotone functions, including nondecreasing, decreasing, and mixed quasimonotone systems. The diffusion terms and time derivatives are discretized using a finite volume method that satisfies the discrete maximum principle (DMP) and the backward Euler method, respectively. The discretization leads to an implicit and nonlinear scheme, and it is proved to preserve the invariant region property unconditionally. We construct an iterative algorithm and prove the invariant region property at each iteration step. Numerical examples are provided to confirm the accuracy and invariant region property of our scheme.

Key words. Reaction-diffusion systems, quasimonotone, nonlinear finite volume scheme, invariant region, distorted meshes, existence, model.

1. Introduction

Reaction-diffusion systems are mathematical models that describe the behaviors of a wide range of physical, biological, chemical, and electrical phenomena [1, 2, 11, 13, 14, 16, 23, 24]. They are used to simulate the variations in chemical substance concentrations caused by local reactions and diffusions in the field of chemistry, the spread of infectious diseases and population growth [5] in biology, the neutron diffusion theory and the Ginzburg-Landau equations for modeling superconductivity [6] in physics, and the FitzHugh-Nagumo model for simulating the transmission of electrical impulses in neurology, among others.

It is of great importance for the numerical methods to preserve the IRP. The IRP refers to the property of reaction-diffusion systems where the solution lies within the range of the initial and boundary values, reflecting the physical constraints of the unknown variables. Hence, the numerical solution is expected to preserve the IRP as well. Additionally, the IRP of numerical schemes is crucial to establishing a prior estimates, as well as existence and stability of the solution [22]. Proposing the IRP-preserving schemes for reaction-diffusion equations is necessary for both physical and mathematical aspects. The finite difference methods [3, 10, 12, 15] have been widely applied to solve the reaction-diffusion equations due to their simplicity. A fully implicit time-discretization method is employed in [12], where the IRP and stability of the scheme are established using M-matrix analysis. In [15], the authors use the exponential time differencing method and overlapping domain decomposition technique to develop a maximum bound principle (MBP) preserving method for one-component reaction-diffusion equations. MBP is considered as a specific form of invariant region. The nonstandard finite difference method together with a time-accurate and highly stable explicit method are combined in [3] to construct a positivity-preserving scheme for the reaction-diffusion model describing vegetation evolution in arid environments. The θ-weighted time-stepping scheme

Received by the editors on March 13, 2024 and, accepted on August 1, 2024.
2000 *Mathematics Subject Classification.* 65M08, 35K58.
*Corresponding author.

and corresponding iterative approach are developed in [10] to solve a class of semilinear parabolic equations. The discrete MBP is preserved under specified constraints on the time step and mesh size. However, most finite difference methods are restricted to rectangular meshes. Furthermore, the finite element method with implicit-explicit Euler time-discretization is utilized to solve 3D reaction-diffusion systems in [9], where the IRP is preserved on Delaunay triangular meshes. The nonlinear Galerkin method is employed in [17] to solve the system of reaction-diffusion equations. This approach requires to calculate the orthonormal basis for the space spanned by the eigenvectors of the diffusion operator. In [25], the finite volume method preserving the IRP is applied to a specific type of reaction-diffusion systems known as FitzHugh-Nagumo equation on polygonal meshes. A unified framework that covers many numerical schemes is established in [7] to yield an MBP-preserving method for semilinear parabolic equations.

The goal of this paper is to propose an IRP-preserving finite volume method solving coupled quasimonotone parabolic systems on distorted meshes. Compared to our previous work in [25], which could only handle specific nonlinear reaction terms, namely $f_1(u,v) = u(1-u)(u-a)-v$ and $f_2(u,v) = \rho u - \gamma v$, this work could handle more general nonlinear reaction terms. We employ the DMP-preserving finite volume scheme to discretize the spatial derivatives and utilize a fully implicit scheme to discretize the temporal derivatives. For the problems with three basic types of quasimonotone functions, we demonstrate that the implicit scheme is unconditionally IRP-preserving and has at least one solution. To solve the nonlinear scheme, we introduce a specific linear term into the iterative algorithm and prove the IRP preservation of the iterative method. Numerical experiments demonstrate that our scheme achieves second-order accuracy in the spatial direction and preserves the IRP for different problems. Additionally, we present a comparison with the nine-point scheme to demonstrate that the nine-point scheme fails to preserve the IRP.

This paper is organized as follows. Section 2 introduces the model problem and its corresponding invariant region theory. Section 3 presents the fully implicit finite volume scheme and analyze the preservation of the IRP. In Section 4, the iterative approach is described and its IRP is analyzed. In Section 5, we provide numerical experiments to demonstrate the accuracy and preservation of the IRP. Finally, Section 6 offers a summary of this paper.

2. Invariant region theory of the model problem

In this paper, we investigate the coupled system of two parabolic equations on a bounded space-time domain $Q_T = \Omega \times (0,T]$ as

$$\partial_t u - \nabla \cdot (\kappa_1 \nabla u) = f_1(u,v), \qquad \text{in } Q_T, \tag{1}$$

$$\partial_t v - \nabla \cdot (\kappa_2 \nabla v) = f_2(u,v), \qquad \text{in } Q_T, \tag{2}$$

subject to the initial conditions $u(\mathbf{x},0) = u_0(\mathbf{x})$ and $v(\mathbf{x},0) = v_0(\mathbf{x})$ on Ω and Dirichlet boundary conditions $u(\mathbf{x},t) = g_1(\mathbf{x},t)$ and $v(\mathbf{x},t) = g_2(\mathbf{x},t)$ on $S_T = \partial\Omega \times (0,T]$. Assume that Ω is an open bounded polygonal domain in $\mathbb{R}^2$, $\partial\Omega \in C^2$, κ_1 and κ_2 are coercive tensor-valued functions, and f_1 and f_2 are nonlinear functions of u and v.

The notations of standard Sobolev spaces are employed, with $(\cdot,\cdot)$ representing the $L^2(Q_T)$ inner product. Define bilinear forms $B_1(u,\phi_1) = (-u\partial_t\phi_1 + \kappa_1\nabla u, \nabla\phi_1)$ and $B_2(v,\phi_2) = (-v\partial_t\phi_2 + \kappa_2\nabla v, \nabla\phi_2)$. We say a pair of functions $(u,v) \in [W_2^{1,1}(Q_T) \bigcap L^\infty(Q_T)]^2$ is a weak solution to the problem (1)-(2) provided that

(i) for any $(\phi_1, \phi_2) \in [\overset{\bullet}{W}{}_2^{1,1}(Q_T)]^2$ and $(\phi_1(\mathbf{x}, T), \phi_2(\mathbf{x}, T)) = 0$ a.e. in Ω, there hold that

$$B_1(u, \phi_1) = (f_1(u, v), \phi_1),$$
$$B_2(v, \phi_2) = (f_2(u, v), \phi_2);$$

(ii) $u(\mathbf{x}, 0) = u_0(\mathbf{x})$, $v(\mathbf{x}, 0) = u_0(\mathbf{x})$ a.e. in Ω in the sense of trace;
(iii) $u(\mathbf{x}, t) = g_1(\mathbf{x}, t)$, $v(\mathbf{x}, t) = g_2(\mathbf{x}, t)$ a.e. on S_T in the sense of trace.

Definition 1. (**Invariant region property**) *A closed set $\Sigma = [m_1, M_1]\times[m_2, M_2]$ in $\mathbb{R}^2$ is called an invariant region of the problem* (1)-(2) *if for almost every (u_0, v_0) and $(g_1, g_2) \in \Sigma$, the corresponding solution $(u, v) \in \Sigma$ for all $0 < t \leq T$.*

The following lemma demonstrates that the quasimonotone reaction-diffusion systems possess the invariant region property under certain hypotheses. The proof can be found in [8].

Lemma 1. *Suppose $\kappa_1, \kappa_2 \in [L^\infty(Q_T)]^{2\times 2}$ are uniformly positive definite in Q_T, $(u_0, v_0) \in [H^1(\Omega)]^2$ and there exists $(G_1, G_2) \in \left[W^{2,1}(Q_T)\right]^2$ such that $(G_1, G_2)|_{S_T} = (g_1, g_2)$. Denote $\Sigma = [m_1, M_1] \times [m_2, M_2]$, where m_1, M_1, m_2, M_2 are constants. Suppose (u_0, v_0) and $(g_1, g_2) \in \Sigma$, $\mathbf{f} = (f_1, f_2)$ is quasimonotone and Lipschitz continuous in Σ and satisfies the following relations*

$$\begin{aligned} &f_1(m_1, v) \geq 0, \quad f_1(M_1, v) \leq 0, \\ &f_2(u, m_2) \geq 0, \quad f_2(u, M_2) \leq 0, \quad \forall (u, v) \in \Sigma, \end{aligned} \tag{3}$$

then, the coupled system (1)-(2) *has a weak solution $(u, v) \in \Sigma$ in $[W_2^{1,1}(Q_T) \bigcap L^\infty(Q_T)]^2$ and is unique in Σ.*

Remark 1. *(i) When $\mathbf{f}$ is quasimonotone nondecreasing, the condition* (3) *is equivalent to $f_1(m_1, m_2) \geq 0, f_1(M_1, M_2) \leq 0, f_2(m_1, m_2) \geq 0, f_2(M_1, M_2) \leq 0$.*

(ii) When $\mathbf{f}$ is quasimonotone nonincreasing, the condition (3) *is equivalent to $f_1(m_1, M_2) \geq 0, f_1(M_1, m_2) \leq 0, f_2(M_1, m_2) \geq 0, f_2(m_1, M_2) \leq 0$.*

(iii) When $\mathbf{f}$ is mixed quasimonotone with nonincreasing f_1 and nondecreasing f_2, the condition (3) *is equivalent to $f_1(m_1, M_2) \geq 0, f_1(M_1, m_2) \leq 0, f_2(m_1, m_2) \geq 0, f_2(M_1, M_2) \leq 0$.*

(iv) When $\mathbf{f}$ is mixed quasimonotone with nondecreasing f_1 and nonincreasing f_2, the condition (3) *is equivalent to $f_1(m_1, m_2) \geq 0, f_1(M_1, M_2) \leq 0, f_2(M_1, m_2) \geq 0, f_2(m_1, M_2) \leq 0$.*

3. The IRP-preserving finite volume scheme

In this section, an IRP-preserving finite volume scheme is constructed to solve the coupled semilinear parabolic equations (1)-(2). The numerical method employs the DMP-preserving finite volume method [21] in space and the backward Euler method in time, resulting in a nonlinear scheme.

In order to present the numerical scheme, it is necessary to introduce the following notations, as indicated in Table 1 and Fig. 1. Define the barycenter of the cell as its cell center. We assume that each polygonal cell is star-shaped with respect to its cell center.

TABLE 1. The notations.

K or L	the cell or the cell center
A or B	the vertex of the cell edge
$m(K)$	the area of cell K
h	the maximum diameter of all cells
σ	the cell edge
$\|\sigma\|$	the length of σ
I	the midpoint of σ
$\mathcal{J}_{in}$	the set of cells
$\mathcal{J}_{out}$	the set of cell edges on $\partial\Omega$
$\mathcal{J}$	$\mathcal{J} = \mathcal{J}_{in} \cup \mathcal{J}_{out}$
$\mathcal{E}_K$	the set of cell edges of K
$\mathcal{E}$	the set of all cell edges
$\mathbf{n}_{K,\sigma}$	the unit outward normal vector on σ of cell K
$\boldsymbol{\tau}_{KI}$ (resp. $\boldsymbol{\tau}_{LI}$)	the unit tangential vector of KI (resp. LI)
$\boldsymbol{\nu}_{KI}$ (resp. $\boldsymbol{\nu}_{LI}$)	the unit normal vector of KI (resp. LI)
$\theta_{K,\sigma}$ (resp. $\theta_{L,\sigma}$)	the angle between vectors $\boldsymbol{\tau}_{KI}$ and $\mathbf{n}_{K,\sigma}$ (resp. $\boldsymbol{\tau}_{LI}$ and $\mathbf{n}_{L,\sigma}$)
t^{n+1}	$t^{n+1} = (n+1)\Delta t$, $\Delta t = \frac{T}{N}$
$\mathcal{F}^{n+1}_{K,\sigma}$ (resp. $\mathcal{F}^{n+1}_{L,\sigma}$)	the continuous normal flux of u on edge σ of the cell K at t^{n+1}(resp. L)
$\tilde{\mathcal{F}}^{n+1}_{K,\sigma}$ (resp. $\tilde{\mathcal{F}}^{n+1}_{L,\sigma}$)	the continuous normal flux of v on edge σ of the cell K at t^{n+1}(resp. L)
$F^{n+1}_{K,\sigma}$ (resp. $F^{n+1}_{L,\sigma}$)	the discrete normal flux of u on edge σ of the cell K at t^{n+1}(resp. L)
$\tilde{F}^{n+1}_{K,\sigma}$ (resp. $\tilde{F}^{n+1}_{L,\sigma}$)	the discrete normal flux of v on edge σ of the cell K at t^{n+1}(resp. L)
$U^{n+1}_X (X = K, L, A, B, I, \cdots)$	the discrete solution U defined at the point X at t^{n+1}
$V^{n+1}_X (X = K, L, A, B, I, \cdots)$	the discrete solution V defined at the point X at t^{n+1}

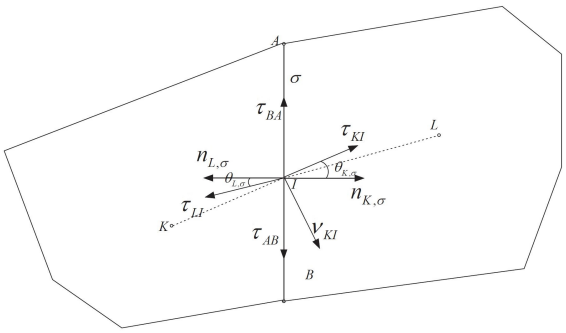

FIGURE 1. The notations.

Integrating the diffusion parts of (1)-(2) over cell K at t^{n+1} and using Green's formula gives

$$-\int_K \nabla\cdot(\kappa_1\nabla u)\big|_{t=t^{n+1}}\mathrm{d}\mathbf{x} = \sum_{\sigma\in\mathcal{E}_K}\mathcal{F}^{n+1}_{K,\sigma},$$
$$-\int_K \nabla\cdot(\kappa_2\nabla v)\big|_{t=t^{n+1}}\mathrm{d}\mathbf{x} = \sum_{\sigma\in\mathcal{E}_K}\tilde{\mathcal{F}}^{n+1}_{K,\sigma},$$

where $\mathcal{F}^{n+1}_{K,\sigma} = -\int_\sigma(\mathbf{n}_{K,\sigma}\cdot\kappa_1^{\mathrm{T}}\nabla u)\big|_{t=t^{n+1}}\mathrm{d}l$ and $\tilde{\mathcal{F}}^{n+1}_{K,\sigma} = -\int_\sigma(\mathbf{n}_{K,\sigma}\cdot\kappa_2^{\mathrm{T}}\nabla v)\big|_{t=t^{n+1}}\mathrm{d}l$ represent the continuous normal flux on edge σ for u and v, respectively.

Next, we give the discretization of $\mathcal{F}^{n+1}_{K,\sigma}$. The discretization of $\tilde{\mathcal{F}}^{n+1}_{K,\sigma}$ is similar and is omitted here. Without ambiguity, the superscript $n+1$ is also omitted in the rest of this section. We employ the DMP-preserving numerical fluxes proposed in [21], which are both nonlinear and conservative.

Let $\boldsymbol{\tau}_{KI}$ and $\mathbf{n}_{K,\sigma}$ denote the unit tangential vector of KI and unit outward normal vector on edge σ of cell K, respectively. Let $\theta_{K,\sigma}$ denote the angle between vectors $\boldsymbol{\tau}_{KI}$ and $\mathbf{n}_{K,\sigma}$. It is obvious that $\theta_{K,\sigma}\in(-\pi/2,\pi/2)$. The vector $\kappa_1^{\mathrm{T}}\mathbf{n}_{K,\sigma}$

can be decomposed into

$$\kappa_1^{\mathrm{T}}\mathbf{n}_{K,\sigma} = -\alpha_K\tau_{BA} + \beta_K\tau_{KI},$$

where

$$\alpha_K := \frac{1}{\cos\theta_{K,\sigma}}\boldsymbol{\nu}_{KI}\cdot\left(\kappa_1^{\mathrm{T}}\mathbf{n}_{K,\sigma}\right), \quad \beta_K := \frac{1}{\cos\theta_{K,\sigma}}\mathbf{n}_{K,\sigma}\cdot\left(\kappa_1^{\mathrm{T}}\mathbf{n}_{K,\sigma}\right).$$

Similarly, we define α_L and β_L. Let $\alpha_{K,\sigma}$, $\alpha_{L,\sigma}$, $\beta_{K,\sigma}$ and $\beta_{L,\sigma}$ denote the integral means of α_K, α_L, β_K and β_L on edge σ, respectively. Since $\theta_{K,\sigma} \in (-\pi/2, \pi/2)$ and κ_1 is coercive, we can infer that $\beta_{K,\sigma} > 0$.

Using Taylor expansion, we obtain

$$\begin{aligned}
\mathcal{F}_{K,\sigma} &= \alpha_{K,\sigma}(u(A) - u(B)) - \frac{|AB|}{|IK|}\beta_{K,\sigma}(u(I) - u(K)) + O(h^2),\\
\mathcal{F}_{L,\sigma} &= \alpha_{L,\sigma}(u(B) - u(A)) - \frac{|AB|}{|IL|}\beta_{L,\sigma}(u(I) - u(L)) + O(h^2).
\end{aligned} \tag{4}$$

The positivity of β_K and β_L implies that $\beta_{K,\sigma} > 0$ and $\beta_{L,\sigma} > 0$.

Utilizing the continuity of normal flux, $\mathcal{F}_{K,\sigma} + \mathcal{F}_{L,\sigma} = 0$ and omitting the $O(h^2)$ terms of $\mathcal{F}_{K,\sigma}$ and $\mathcal{F}_{L,\sigma}$, we derive the expression for $u(I)$. Subsequently, substituting $u(I)$ into (4) leads to

$$\begin{aligned}
\mathcal{F}_{K,\sigma} &= \tau_\sigma(u(K) - u(L)) + \tau_\sigma D_\sigma(u(A) - u(B)) + O(h^2),\\
\mathcal{F}_{L,\sigma} &= \tau_\sigma(u(L) - u(K)) + \tau_\sigma D_\sigma(u(B) - u(A)) + O(h^2),
\end{aligned} \tag{5}$$

where $\tau_\sigma = \frac{|AB|}{\frac{|IK|}{\beta_{K,\sigma}} + \frac{|IL|}{\beta_{L,\sigma}}}$, $D_\sigma = \frac{|IK|\alpha_{K,\sigma}}{|AB|\beta_{K,\sigma}} + \frac{|IL|\alpha_{L,\sigma}}{|AB|\beta_{L,\sigma}}$. It can be observed that $\tau_\sigma > 0$ due to the fact that $\beta_K > 0$. However, D_σ, with its sign being dependent on the diffusion tensor and the geometry of the cell.

Using the second-order method in [18] to approximate the vertex unknowns $u(A)$ and $u(B)$, it follows that

$$\begin{aligned}
u(A) &= \sum_{i=1}^{J_A}\omega_{A_i}u(K_{A_i}),\\
u(B) &= \sum_{i=1}^{J_B}\omega_{B_i}u(K_{B_i}),
\end{aligned}$$

where K_{A_i} denotes the cell-centered unknowns involved in the approximation of $u(A)$, and J_A denotes the number of K_{A_i}. Similarly, we define K_{B_i} and J_B. The weighted coefficients satisfy $\sum_{i=1}^{J_A}\omega_{A_i} = 1$ and $\sum_{i=1}^{J_B}\omega_{B_i} = 1$, and they are not restricted to being nonnegative.

Substituting the expressions of $u(A)$ and $u(B)$ into (5) yields the following expressions

$$\begin{aligned}
\mathcal{F}_{K,\sigma} &= \tau_\sigma(u(K) - u(L)) + \tau_\sigma D_\sigma\left(\sum_{i=1}^{J_A}\omega_{A_i}u(K_{A_i}) - \sum_{i=1}^{J_B}\omega_{B_i}u(K_{B_i})\right) + O(h^2),\\
\mathcal{F}_{L,\sigma} &= \tau_\sigma(u(L) - u(K)) - \tau_\sigma D_\sigma\left(\sum_{i=1}^{J_A}\omega_{A_i}u(K_{A_i}) - \sum_{i=1}^{J_B}\omega_{B_i}u(K_{B_i})\right) + O(h^2).
\end{aligned}$$

Denote by $F_{K,\sigma}^{NP}$ and $F_{L,\sigma}^{NP}$ as the numerical fluxes of the nine-point scheme [18], we have

$$\begin{aligned} F_{K,\sigma}^{NP} &= \tau_\sigma(U_K - U_L) + \Delta_\sigma, \\ F_{L,\sigma}^{NP} &= \tau_\sigma(U_L - U_K) - \Delta_\sigma, \end{aligned} \tag{6}$$

where $\Delta_\sigma = \tau_\sigma D_\sigma \left(\sum_{i=1}^{J_A} \omega_{A_i} U_{K_{A_i}} - \sum_{i=1}^{J_B} \omega_{B_i} U_{K_{B_i}} \right)$, and U denotes the discrete solution.

Denote U_{K_1} and U_{K_2} such that

$$\begin{aligned} U_{K_1} &= \min_{\bar{K} \in \mathcal{J}_K} U_{\bar{K}}, \\ U_{K_2} &= \max_{\bar{K} \in \mathcal{J}_K} U_{\bar{K}}, \end{aligned} \tag{7}$$

where $\mathcal{J}_K$ denotes the set of cells that have common vertices with cell K except for K.

In the numerical algorithm, we introduce two small positive constants ε_0 and ε_1, where $\varepsilon_0, \varepsilon_1 \le Ch^2$. For our numerical experiments, we choose $\varepsilon_0 = \varepsilon_1 = 10^{-10}$.

If $|\Delta_\sigma| \le \varepsilon_0$, we define the numerical fluxes as follows:

$$\begin{aligned} F_{K,\sigma} &= \tau_\sigma \left(U_K - U_L \right), \\ F_{L,\sigma} &= \tau_\sigma \left(U_L - U_K \right). \end{aligned}$$

If $|\Delta_\sigma| > \varepsilon_0$, then the construction contains two cases:

Case 1. There exist $U_{K'}$ and $U_{L'}$ such that

$$\begin{aligned} \Delta_\sigma(U_K - U_{K'}) > 0, \\ \Delta_\sigma(U_{L'} - U_L) > 0, \end{aligned} \tag{8}$$

where $U_{K'}$ and $U_{L'}$ are the cell-centered unknowns surrounding K and L, respectively. $U_{K'}$ and $U_{L'}$ can be taken as U_{K_1} or U_{K_2} in (7). In this case, the numerical fluxes are defined as

$$\begin{aligned} F_{K,\sigma} &= \tau_\sigma \left(U_K - U_L \right) + \eta_{K,\sigma}(U_K - U_{K'}), \\ F_{L,\sigma} &= \tau_\sigma \left(U_L - U_K \right) + \eta_{L,\sigma}(U_L - U_{L'}), \end{aligned}$$

where $\eta_{K,\sigma} = \frac{\Delta_\sigma}{U_K - U_{K'}}$ and $\eta_{L,\sigma} = \frac{\Delta_\sigma}{U_{L'} - U_L}$. It can be observed that the nonlinear coefficients $\eta_{K,\sigma} > 0$ and $\eta_{L,\sigma} > 0$ since Δ_σ and $U_K - U_{K'}$, $U_{L'} - U_L$ are of the same sign in this case.

Case 2. There do not exist $U_{K'}$ and $U_{L'}$ such that (8) holds. It is equivalent to

$$\Delta_\sigma(U_K - U_{K'}) \le 0 \tag{9}$$

for any $K' \in \mathcal{J}_K$, or

$$\Delta_\sigma(U_{L'} - U_L) \le 0 \tag{10}$$

for any $L' \in \mathcal{J}_L$. It implies that U reaches its maximum or minimum on cell K or L, and from (9) and (10) we have

$$\Delta_\sigma(U_K - U_L) \le 0. \tag{11}$$

Rewrite the linear numerical fluxes (6) as

$$\begin{aligned} F_{K,\sigma}^{NP} &= (1 - \gamma_0)\tau_\sigma \left(U_K - U_L \right) + \Delta_\sigma + \gamma_0 \tau_\sigma (U_K - U_L), \\ F_{L,\sigma}^{NP} &= (1 - \gamma_0)\tau_\sigma \left(U_L - U_K \right) - \Delta_\sigma + \gamma_0 \tau_\sigma (U_L - U_K), \end{aligned}$$

where γ_0 is a nonlinear coefficient determined later. To preserve the IRP, the numerical flux needs to satisfy the DMP structure, i.e., the numerical flux should be the convex combinations of $U_K - U_{K_j}$. To guarantee $1-\gamma_0 > 0$, the coefficient γ_0 should satisfy

$$0 \le \gamma_0 \le 1 - \varepsilon_1.$$

In this case, we define the final nonlinear numerical fluxes:

$$F_{K,\sigma} = (1-\gamma_0)\tau_\sigma\left(U_K - U_L\right),$$
$$F_{L,\sigma} = (1-\gamma_0)\tau_\sigma\left(U_L - U_K\right).$$

If $|U_K - U_L| = 0$, we set $\gamma_0 = 1-\varepsilon_1$, otherwise, we set

$$\gamma_0 = \begin{cases} \dfrac{-\Delta_\sigma}{\tau_\sigma\left(U_K - U_L\right)}, & \text{if } \dfrac{-\Delta_\sigma}{\tau_\sigma\left(U_K - U_L\right)} \le 1-\varepsilon_1, \\ 1-\varepsilon_1, & \text{else.} \end{cases}$$

The inequality (11) guarantees the nonnegativity of γ_0.

Up to now, we have constructed the numerical flux with a DMP-preserving structure, where the numerical flux is conservative and nonlinear.

Remark 2. *This paper presents a DMP-preserving finite volume method in* [21] *for the discretization of the diffusion term. It's important to note that the choice of discretization is flexible. As long as the discretization of the diffusion term is a DMP-preserving finite volume scheme (for example, the methods provided in* [4, 19, 20]*), the invariant region analysis in this paper is valid.*

To discretize the time derivative, we utilize the Backward Euler method. Hence, we obtain the nonlinear finite volume scheme (12)-(17):

$$m(K)\frac{U_K^{n+1} - U_K^n}{\Delta t} + \sum_{\sigma\in\mathcal{E}_K} F_{K,\sigma}^{n+1} = m(K) f_1(U_K^{n+1}, V_K^{n+1}),\ \forall K \in \mathcal{J}_{in}, \tag{12}$$

$$m(K)\frac{V_K^{n+1} - V_K^n}{\Delta t} + \sum_{\sigma\in\mathcal{E}_K} \tilde{F}_{K,\sigma}^{n+1} = m(K) f_2(U_K^{n+1}, V_K^{n+1}),\ \forall K \in \mathcal{J}_{in}, \tag{13}$$

$$U_K^{n+1} = g_1(K, t^{n+1}), \qquad \forall K \in \mathcal{J}_{out}, \tag{14}$$

$$V_K^{n+1} = g_2(K, t^{n+1}), \qquad \forall K \in \mathcal{J}_{out}, \tag{15}$$

$$U_K^0 = u_0(K), \qquad \forall K \in \mathcal{J}_{in} \cup \mathcal{J}_{out}, \tag{16}$$

$$V_K^0 = v_0(K), \qquad \forall K \in \mathcal{J}_{in} \cup \mathcal{J}_{out}. \tag{17}$$

We demonstrate that the finite volume scheme (12)-(17) can preserve the IRP for the semilinear parabolic systems with three basic types of quasimonotone functions, as shown in Theorem 1 and Theorem 2.

Theorem 1. *Assume that* $\mathbf{f} = (f_1, f_2)$ *satisfies* (3) *and is mixed quasimonotone and Lipschitz continuous in* $\Sigma = [m_1, M_1] \times [m_2, M_2]$ *with Lipschitz constant* λ*. Assume further that the initial and boundary conditions satisfy* $(u_0, v_0), (g_1, g_2) \in \Sigma$*. When the time-step size* $\Delta t < \dfrac{1}{\lambda}$*, the finite volume scheme* (12)-(17) *has a solution satisfying*

$$(U_K^n, V_K^n) \in \Sigma, \quad \forall K \in \mathcal{J}, \quad 0 \le n \le N. \tag{18}$$

Proof. This theorem is proved by induction. For mixed quasimonotone reaction-diffusion systems, we only prove the theorem in the case where f_1 is quasimonotone nonincreasing and f_2 is quasimonotone nondecreasing; the other case can be proved similarly. Since (u_0, v_0), $(g_1, g_2) \in \Sigma$, it is obvious that (18) holds for $n = 0$. Suppose that (18) holds for any $n \le m$, if (18) is proved for $n = m + 1$, where $m \ge 0$, then the theorem follows immediately.

First, construct the prolongation functions $\bar{f}_1(u_1, u_2)$ and $\bar{f}_2(u_1, u_2)$ as follows. For any $u_1 \in \mathbb{R}$ and $u_2 \in \mathbb{R}$, define

$$\bar{f}_1(u_1, u_2) = \begin{cases} f_1(u_1, m_2), & \text{if } u_2 < m_2, \\ f_1(u_1, u_2), & \text{if } m_2 \le u_2 \le M_2, \\ f_1(u_1, M_2), & \text{if } u_2 > M_2. \end{cases}$$

and

$$\bar{f}_2(u_1, u_2) = \begin{cases} f_2(m_1, u_2), & \text{if } u_1 < m_1, \\ f_2(u_1, u_2), & \text{if } m_1 \le u_1 \le M_1, \\ f_2(M_1, u_2), & \text{if } u_1 > M_1. \end{cases}$$

Note that $(\bar{f}_1, \bar{f}_2)$ is also mixed quasimonotone in $\mathbb{R}^2$. It is easy to check that $\bar{f}_1$ and $\bar{f}_2$ are Lipschitz continuous in $\mathbb{R}^2$ and λ is still the Lipschitz constant of $\bar{f}_1$ and $\bar{f}_2$, and there hold

$$\bar{f}_1(M_1, m_2) \le 0 \le \bar{f}_1(m_1, M_2),$$
$$\bar{f}_2(M_1, M_2) \le 0 \le \bar{f}_2(m_1, m_2).$$

Next, for a given $(U^m, V^m) \in \Sigma$, denote $(\bar{U}^{m+1}, \bar{V}^{m+1})$ as the solution to the following problem:

$$m(K)\frac{\bar{U}_K^{m+1} - U_K^m}{\Delta t} + \sum_{\sigma \in \mathcal{E}_K} F_{K,\sigma}^{m+1} = m(K)\bar{f}_1(\bar{U}_K^{m+1}, \bar{V}_K^{m+1}), \quad \forall K \in \mathcal{J}_{in}, \tag{19}$$

$$m(K)\frac{\bar{V}_K^{m+1} - V_K^m}{\Delta t} + \sum_{\sigma \in \mathcal{E}_K} \tilde{F}_{K,\sigma}^{m+1} = m(K)\bar{f}_2(\bar{U}_K^{m+1}, \bar{V}_K^{m+1}), \quad \forall K \in \mathcal{J}_{in}, \tag{20}$$

$$\bar{U}_K^{m+1} = g_1(K, t^{m+1}), \quad \forall K \in \mathcal{J}_{out}, \tag{21}$$

$$\bar{V}_K^{m+1} = g_2(K, t^{m+1}), \quad \forall K \in \mathcal{J}_{out}, \tag{22}$$

where $F_{K,\sigma}^{m+1}$ and $\tilde{F}_{K,\sigma}^{m+1}$ are constructed by $\bar{U}_K^{m+1}$ and $\bar{V}_K^{m+1}$.

Denote $K_{\max,U}$, $K_{\min,U}$, $K_{\max,V}$, $K_{\min,V}$ such that

$$\bar{U}_{K_{\max,U}}^{m+1} = \max_{K \in \mathcal{J}} \bar{U}_K^{m+1}, \quad \bar{U}_{K_{\min,U}}^{m+1} = \min_{K \in \mathcal{J}} \bar{U}_K^{m+1},$$
$$\bar{V}_{K_{\max,V}}^{m+1} = \max_{K \in \mathcal{J}} \bar{V}_K^{m+1}, \quad \bar{V}_{K_{\min,V}}^{m+1} = \min_{K \in \mathcal{J}} \bar{V}_K^{m+1}.$$

If (18) does not hold for $n = m + 1$, then one of the following cases holds:

$$\text{Case 1: } \bar{U}_{K_{\max,U}}^{m+1} > M_1. \quad \text{Case 2: } \bar{U}_{K_{\min,U}}^{m+1} < m_1.$$
$$\text{Case 3: } \bar{V}_{K_{\max,V}}^{m+1} > M_2. \quad \text{Case 4: } \bar{V}_{K_{\min,V}}^{m+1} < m_2.$$

We shall prove by contradiction that none of the above cases hold true. Let us suppose Case 1 holds. Since $\bar{U}^{m+1}$ attains its maximum on $K_{\max,U}$ and the numerical flux has DMP-preserving structure, it follows that $F_{K_{\max,U},\sigma}^{m+1} \le 0$ for any

$\sigma \in \mathcal{E}_{K_{\max,U}}$. From $U^m_{K_{\max,U}} \in [m_1, M_1]$ and (12), we can get

$$\frac{\bar{U}^{m+1}_{K_{\max,U}} - M_1}{\Delta t} \le \frac{\bar{U}^{m+1}_{K_{\max,U}} - U^m_{K_{\max,U}}}{\Delta t} \le \bar{f}_1(\bar{U}^{m+1}_{K_{\max,U}}, \bar{V}^{m+1}_{K_{\max,U}}). \tag{23}$$

(A) $\bar{V}^{m+1}_{K_{\max,U}} \ge m_2$.

Since $\bar{f}_1$ is nonincreasing with respect to v, we have $\bar{f}_1(M_1, \bar{V}^{m+1}_{K_{\max,U}}) \le \bar{f}_1(M_1, m_2) \le 0$. According to (23) and Lipschitz continuity of $\bar{f}_1$, we have

$$\begin{aligned}\frac{\bar{U}^{m+1}_{K_{\max,U}} - M_1}{\Delta t} &\le \bar{f}_1(\bar{U}^{m+1}_{K_{\max,U}}, \bar{V}^{m+1}_{K_{\max,U}}) - \bar{f}_1(M_1, \bar{V}^{m+1}_{K_{\max,U}}) \\ &\le \lambda(\bar{U}^{m+1}_{K_{\max,U}} - M_1).\end{aligned} \tag{24}$$

When $\Delta t < \dfrac{1}{\lambda}$, (24) implies that $\bar{U}^{m+1}_{K_{\max,U}} \le M_1$, which contradicts the assumption that $\bar{U}^{m+1}_{K_{\max,U}} > M_1$.

(B) $\bar{V}^{m+1}_{K_{\max,U}} < m_2$.

From $\bar{V}^{m+1}_{K_{\max,U}} < m_2$, we have $\bar{V}^{m+1}_{K_{\min,V}} < m_2$. Since $\bar{V}^{m+1}$ attains its minimum on $K_{\min,V}$, similar to (23), we can obtain

$$\frac{\bar{V}^{m+1}_{K_{\min,V}} - m_2}{\Delta t} \ge \frac{\bar{V}^{m+1}_{K_{\min,V}} - \bar{V}^m_{K_{\min,V}}}{\Delta t} \ge \bar{f}_2(\bar{U}^{m+1}_{K_{\min,V}}, \bar{V}^{m+1}_{K_{\min,V}}). \tag{25}$$

(B.1) $\bar{U}^{m+1}_{K_{\min,V}} \ge m_1$.

Since $\bar{f}_2$ is nondecreasing with respect to u, we have $\bar{f}_2(\bar{U}^{m+1}_{K_{\min,U}}, m_2) \ge \bar{f}_2(m_1, m_2) \ge 0$. Similar to the derivation of (24), it follows that

$$\frac{\bar{V}^{m+1}_{K_{\min,V}} - m_2}{\Delta t} \ge \bar{f}_2(\bar{U}^{m+1}_{K_{\min,V}}, \bar{V}^{m+1}_{K_{\min,V}}) - \bar{f}_2(\bar{U}^{m+1}_{K_{\min,U}}, m_2) \ge \lambda(\bar{V}^{n+1}_{K_{\min,V}} - m_2). \tag{26}$$

When $\Delta t < \dfrac{1}{\lambda}$, (26) implies $\bar{V}^{m+1}_{K_{\min,V}} \ge m_2$, which contradicts $\bar{V}^{m+1}_{K_{\min,V}} < m_2$.

(B.2) $\bar{U}^{m+1}_{K_{\min,V}} < m_1$.

The assumption $\bar{U}^{m+1}_{K_{\min,V}} < m_1$ implies $\bar{U}^{m+1}_{K_{\min,U}} < m_1$. Since $\bar{U}^{m+1}$ attains its minimum on $K_{\min,U}$, we can obtain

$$\begin{aligned}\frac{\bar{U}^{m+1}_{K_{\min,U}} - m_1}{\Delta t} &\ge \frac{\bar{U}^{m+1}_{K_{\min,U}} - U^m_{K_{\min,U}}}{\Delta t} \\ &\ge \bar{f}_1(\bar{U}^{m+1}_{K_{\min,U}}, \bar{V}^{m+1}_{K_{\min,U}}).\end{aligned} \tag{27}$$

(B.2.a) $\bar{V}^{m+1}_{K_{\min,U}} \le M_2$.

Since $\bar{f}_1$ is nonincreasing with respect to v, we have $\bar{f}_1(m_1, \bar{V}^{m+1}_{K_{\min,U}}) \ge \bar{f}_1(m_1, M_2) \ge 0$. According to (27) and the Lipschitz continuity of $\bar{f}_1$, we have

$$\frac{\bar{U}^{m+1}_{K_{\min,U}} - m_1}{\Delta t} \ge \bar{f}_1(\bar{U}^{m+1}_{K_{\min,U}}, \bar{V}^{m+1}_{K_{\min,U}}) - \bar{f}_1(m_1, \bar{V}^{m+1}_{K_{\min,U}}) \ge \lambda(\bar{U}^{m+1}_{K_{\min,U}} - m_1),$$

which means that $\bar{U}^{m+1}_{K_{\min,U}} \ge m_1$ when $\Delta t < \dfrac{1}{\lambda}$. This contradicts $\bar{U}^{m+1}_{K_{\min,U}} < m_1$.

(B.2.b) $\bar{V}^{m+1}_{K_{\min,U}} > M_2$.

The assumption $\bar{V}^{m+1}_{K_{\min,U}} > M_2$ implies $\bar{V}^{m+1}_{K_{\max,V}} > M_2$. Since $\bar{V}^{m+1}$ attains its maximum on $K_{\max,V}$, similar to (23), we can obtain

$$\frac{\bar{V}^{m+1}_{K_{\max,V}} - M_2}{\Delta t} \le \frac{\bar{V}^{m+1}_{K_{\max,V}} - V^m_{K_{\max,V}}}{\Delta t} \le \bar{f}_2(\bar{U}^{m+1}_{K_{\max,V}}, \bar{V}^{m+1}_{K_{\max,V}}). \tag{28}$$

(B.2.b(i)) $\bar{U}^{m+1}_{K_{\max,V}} \le M_1$.

Since $\bar{f}_2$ is nondecreasing with respect to u, we have $\bar{f}_2(\bar{U}^{m+1}_{K_{\max,V}}, M_2) \le \bar{f}_2(M_1, M_2) \le 0$. According to (28) and the Lipschitz continuity of $\bar{f}_2$, we have

$$\begin{aligned} \frac{\bar{V}^{m+1}_{K_{\max,V}} - M_2}{\Delta t} &\le \bar{f}_2(\bar{U}^{m+1}_{K_{\max,V}}, \bar{V}^{m+1}_{K_{\max,V}}) - \bar{f}_2(\bar{U}^{m+1}_{K_{\max,V}}, M_2) \\ &\le \lambda(\bar{V}^{m+1}_{K_{\max,V}} - M_2), \end{aligned} \tag{29}$$

which means $\bar{V}^{m+1}_{K_{\max,V}} \le M_2$ provided that $\Delta t < \dfrac{1}{\lambda}$. This contradicts $\bar{V}^{m+1}_{K_{\max,V}} > M_2$.

(B.2.b(ii)) $\bar{U}^{m+1}_{K_{\max,V}} > M_1$.

Since $\bar{f}_1$ is nonincreasing with respect to v and $\bar{V}^{m+1}_{K_{\max,U}} > M_2 > m_2$, we have $\bar{f}_1(M_1, \bar{V}^{m+1}_{K_{\max,U}}) \le \bar{f}_1(M_1, m_2) \le 0$. Similar to the derivation of (24), it holds that

$$\frac{\bar{U}^{m+1}_{K_{\max,U}} - M_1}{\Delta t} \le \lambda(\bar{U}^{m+1}_{K_{\max,U}} - M_1),$$

which implies $\bar{U}^{m+1}_{K_{\max,U}} \le M_1$ provided that $\Delta t < \dfrac{1}{\lambda}$. This contradicts $\bar{U}^{m+1}_{K_{\max,U}} > M_1$.

In conclusion, Case 1 does not hold provided that $\Delta t < \dfrac{1}{\lambda}$. Similarly, the other cases do not hold when $\Delta t < \dfrac{1}{\lambda}$. Hence $(\bar{U}^{m+1}_K, \bar{V}^{m+1}_K) \in \Sigma$ for any $K \in \mathcal{J}_{in} \cup \mathcal{J}_{out}$, it follows that $\bar{f}_1(\bar{U}^{m+1}_K, \bar{V}^{m+1}_K) = f_1(\bar{U}^{m+1}_K, \bar{V}^{m+1}_K)$, $\bar{f}_2(\bar{U}^{m+1}_K, \bar{V}^{m+1}_K) = f_2(\bar{U}^{m+1}_K, \bar{V}^{m+1}_K)$. We obtain that $(\bar{U}^{m+1}_K, \bar{V}^{m+1}_K) \in \Sigma$ is also the solution of following scheme

$$\begin{aligned} m(K)\frac{U^{m+1}_K - U^m_K}{\Delta t} + \sum_{\sigma\in\mathcal{E}_K} F^{m+1}_{K,\sigma} &= m(K) f_1(U^{m+1}_K, V^{m+1}_K), && \forall K \in \mathcal{J}_{in}, \\ m(K)\frac{V^{m+1}_K - V^m_K}{\Delta t} + \sum_{\sigma\in\mathcal{E}_K} \tilde{F}^{m+1}_{K,\sigma} &= m(K) f_2(U^{m+1}_K, V^{m+1}_K), && \forall K \in \mathcal{J}_{in}, \\ U^{m+1}_K &= g_1(K, t^{m+1}), && \forall K \in \mathcal{J}_{out}, \\ V^{m+1}_K &= g_2(K, t^{m+1}), && \forall K \in \mathcal{J}_{out}, \end{aligned}$$

which means that the finite volume scheme (12)-(17) has a solution (U^{m+1}, V^{m+1}) in the invariant region. This completes the proof. □

We shall now demonstrate that the finite volume scheme can preserve the IRP for the semilinear parabolic systems with quasimonotone nondecreasing reaction function. The same method can be applied for the case of a quasimonotone nonincreasing reaction function, which we will omit for brevity.

Theorem 2. *Assume that* $\mathbf{f} = (f_1, f_2)$ *satisfies* (3) *and is quasimonotone nondecreasing (or vice versa) and Lipschitz continuous in* $\Sigma = [m_1, M_1] \times [m_2, M_2]$, *the initial and boundary conditions satisfy* $(u_0, v_0), (g_1, g_2) \in \Sigma$. *When* $\Delta t < \dfrac{1}{2\lambda}$, *the*

finite volume scheme has a solution satisfying

$$(U_K^n, V_K^n) \in \Sigma, \quad \forall K \in \mathcal{J}, \quad 0 \le n \le N. \tag{30}$$

Proof. We shall adopt the same procedure as in the proof of Theorem 1. It is obvious that (30) holds for $n = 0$. Suppose that (30) holds for any $n \le m$, where $m \ge 0$. Our objective is to demonstrate that (30) holds for $n = m + 1$.

The definitions of prolongation functions $\bar{f}_1(u_1, u_2)$ and $\bar{f}_2(u_1, u_2)$ are the same as in the proof of Theorem 1, and $(\bar{f}_1, \bar{f}_2)$ is also quasimonotone nondecreasing in $\mathbb{R}^2$ and satisfies

$$\bar{f}_1(M_1, M_2) \le 0 \le \bar{f}_1(m_1, m_2),$$
$$\bar{f}_2(M_1, M_2) \le 0 \le \bar{f}_2(m_1, m_2).$$

Similar to the proof of Theorem 1, we define $(\bar{U}^{m+1}, \bar{V}^{m+1})$ as the solution of the finite volume scheme corresponding to $(\bar{f}_1, \bar{f}_2)$. The definitions of $K_{\max,U}$, $K_{\min,U}$, $K_{\max,V}$ and $K_{\min,V}$ are also the same as those in Theorem 1.

Suppose that (30) does not hold for $n = m + 1$, then one of the following cases holds:

$$\text{Case 1: } \bar{U}^{m+1}_{K_{\max,U}} > M_1. \quad \text{Case 2: } \bar{U}^{m+1}_{K_{\min,U}} < m_1.$$
$$\text{Case 3: } \bar{V}^{m+1}_{K_{\max,V}} > M_2. \quad \text{Case 4: } \bar{V}^{m+1}_{K_{\min,V}} < m_2.$$

Let us suppose Case 1 holds. We can obtain that (23) holds since $\bar{U}^{m+1}$ attains its maximum on $K_{\max,U}$.

(A) $\bar{V}^{m+1}_{K_{\max,U}} \le M_2$.

Since $\bar{f}_1$ is nondecreasing with respect to v, we have $\bar{f}_1(M_1, \bar{V}^{m+1}_{K_{\max,U}}) \le \bar{f}_1(M_1, M_2) \le 0$. Similar to the derivation of (24), we obtain

$$\frac{\bar{U}^{m+1}_{K_{\max,U}} - M_1}{\Delta t} \le \lambda(\bar{U}^{m+1}_{K_{\max,U}} - M_1). \tag{31}$$

(31) implies $\bar{U}^{m+1}_{K_{\max,U}} \le M_1$ provided that $\Delta t < \dfrac{1}{\lambda}$, which contradicts the assumption of Case 1.

(B) $\bar{V}^{m+1}_{K_{\max,U}} > M_2$.

The assumption $\bar{V}^{m+1}_{K_{\max,U}} > M_2$ implies $\bar{V}^{m+1}_{K_{\max,V}} > M_2$. It follows that (28) since $\bar{V}^{m+1}_{K_{\max,V}}$ is the maximum of $\bar{V}^{m+1}$.

(B.1) $\bar{U}^{m+1}_{K_{\max,V}} \le M_1$.

Since $\bar{f}_2$ is nondecreasing with respect to u, we have $\bar{f}_2(\bar{U}^{m+1}_{K_{\max,V}}, M_2) \le \bar{f}_2(M_1, M_2) \le 0$. Similar to the derivation of (29), we have

$$\frac{\bar{V}^{m+1}_{K_{\max,V}} - M_2}{\Delta t} \le \lambda(\bar{V}^{m+1}_{K_{\max,V}} - M_2). \tag{32}$$

When $\Delta t < \dfrac{1}{\lambda}$, (32) implies that $\bar{V}^{m+1}_{K_{\max,V}} \le M_2$, which contradicts $\bar{V}^{m+1}_{K_{\max,U}} > M_2$.

(B.2) $\bar{U}^{m+1}_{K_{\max,V}} > M_1$.

The assumption $\bar{U}^{m+1}_{K_{\max,V}} > M_1$ implies that $\bar{U}^{m+1}_{K_{\max,U}} > M_1$. From the Lipschitz continuity of $\bar{f}_1$ and $\bar{f}_1(M_1, M_2) \ge 0$, it follows that

$$\frac{\bar{U}^{m+1}_{K_{\max,U}} - M_1}{\Delta t} \le \lambda(\bar{U}^{m+1}_{K_{\max,U}} - M_1) + \lambda(\bar{V}^{m+1}_{K_{\max,U}} - M_2). \tag{33}$$

From (33), we can obtain

$$\bar{U}^{m+1}_{K_{\max,U}} - M_1 \le \frac{\lambda\Delta t}{1-\lambda\Delta t}(\bar{V}^{m+1}_{K_{\max,U}} - M_2). \tag{34}$$

Similar to the derivations of (33) and (34), $\bar{V}^{m+1}_{K_{\max,V}}$ satisfies the following inequalities

$$\begin{aligned}\frac{\bar{V}^{m+1}_{K_{\max,U}} - M_2}{\Delta t} &\le \bar{f}_2(\bar{U}^{m+1}_{K_{\max,V}}, \bar{V}^{m+1}_{K_{\max,V}}) - \bar{f}_2(M_1, M_2)\\ &\le \lambda(\bar{U}^{m+1}_{K_{\max,V}} - M_1) + \lambda(\bar{V}^{m+1}_{K_{\max,V}} - M_2),\end{aligned}$$

and

$$\bar{U}^{m+1}_{K_{\max,V}} - M_1 \ge \frac{1-\lambda\Delta t}{\lambda\Delta t}(\bar{V}^{m+1}_{K_{\max,V}} - M_2). \tag{35}$$

Combining (34) and (35), we see that $\frac{\lambda\Delta t}{1-\lambda\Delta t}(\bar{V}^{m+1}_{K_{\max,U}} - M_2) \ge \frac{1-\lambda\Delta t}{\lambda\Delta t}(\bar{V}^{m+1}_{K_{\max,V}} - M_2)$. We have $\frac{\lambda\Delta t}{1-\lambda\Delta t} > \frac{1-\lambda\Delta t}{\lambda\Delta t}$ provided that $\Delta t < \frac{1}{2\lambda}$, which derives that $\bar{V}^{m+1}_{K_{\max,U}} \le M_2$. It contradicts the assumption that $\bar{V}^{m+1}_{K_{\max,U}} > M_2$. Hence, Case 1 does not hold when $\Delta t < \frac{1}{2\lambda}$. The proofs of other cases follow similarly.

In conclusion, we have proved that $(\bar{U}^{m+1}_K, \bar{V}^{m+1}_K) \in \Sigma$ for any $K \in \mathcal{J}_{in} \cup \mathcal{J}_{out}$, then we have $\bar{f}_1(\bar{U}^{m+1}_K, \bar{V}^{m+1}_K) = f_1(\bar{U}^{m+1}_K, \bar{V}^{m+1}_K)$ and $\bar{f}_2(\bar{U}^{m+1}_K, \bar{V}^{m+1}_K) = f_2(\bar{U}^{m+1}_K, \bar{V}^{m+1}_K)$. It means that $(\bar{U}^{m+1}, \bar{V}^{m+1})$ is also the solution of the finite volume scheme (12)-(17), which completes the proof. □

The existence of a solution for the nonlinear finite volume scheme (12)-(17) can be established using the same method as Theorem 4 in [25], and this proof is therefore omitted.

Theorem 3. *Suppose that* $\mathbf{f} = (f_1, f_2)$ *is quasimonotone and Lipschitz continuous in* $\Sigma = [m_1, M_1] \times [m_2, M_2]$*, and satisfies* (3)*, the initial and boundary conditions satisfy* $(u_0, v_0), (g_1, g_2) \in \Sigma$*. When* $\Delta t < \frac{1}{2\lambda}$*, the nonlinear finite volume scheme* (12)-(17) *has at least one solution.*

4. The iterative method preserving the IRP

In this section, we design an iterative method to solve the nonlinear scheme (12)-(17) and then prove the IRP of the iteration. To design the iterative scheme, we first linearize the nonlinear numerical flux. Denote $U^{n+1,s+1}$ and $V^{n+1,s+1}$ the $(s+1)$-th iterative numerical solutions at t^{n+1}. We use the solution $U^{n+1,s}$ to calculate the coefficients $\eta^{n+1,s}_{K,\sigma}$, $\eta^{n+1,s}_{L,\sigma}$, $\gamma^{n+1,s}_0$ and $\Delta^{n+1,s}_\sigma$. For Case 1 in the algorithm, the numerical flux $F^{n+1,s+1}_{K,\sigma}$ and $F^{n+1,s+1}_{L,\sigma}$ are defined as

$$\begin{aligned}F^{n+1,s+1}_{K,\sigma} &= \tau^{n+1}_\sigma\left(U^{n+1,s+1}_K - U^{n+1,s+1}_L\right) + \eta^{n+1,s}_{K,\sigma}\left(U^{n+1,s+1}_K - U^{n+1,s+1}_{K'}\right),\\ F^{n+1,s+1}_{L,\sigma} &= \tau^{n+1}_\sigma\left(U^{n+1,s+1}_L - U^{n+1,s+1}_K\right) + \eta^{n+1,s}_{L,\sigma}\left(U^{n+1,s+1}_L - U^{n+1,s+1}_{L'}\right),\end{aligned}$$

and for Case 2, $F^{n+1,s+1}_{K,\sigma}$ and $F^{n+1,s+1}_{L,\sigma}$ are defined as

$$\begin{aligned}F^{n+1,s+1}_{K,\sigma} &= (1-\gamma^{n+1,s}_0)\tau^{n+1}_\sigma\left(U^{n+1,s+1}_K - U^{n+1,s+1}_L\right),\\ F^{n+1,s+1}_{L,\sigma} &= (1-\gamma^{n+1,s}_0)\tau^{n+1}_\sigma\left(U^{n+1,s+1}_L - U^{n+1,s+1}_K\right).\end{aligned}$$

Similarly, we define $\tilde{F}_{K,\sigma}^{n+1,s+1}$ and $\tilde{F}_{L,\sigma}^{n+1,s+1}$.

The treatment of the nonlinear source term is crucial for preserving IRP during the iteration. For given $U^{n+1,s}$ and $V^{n+1,s}$, the solution of the iteration $(U^{n+1,s+1}, V^{n+1,s+1})$ satisfies

$$\begin{aligned} &m(K)\frac{U_K^{n+1,s+1}-U_K^n}{\Delta t}+\sum_{\sigma\in\mathcal{E}_K}F_{K,\sigma}^{n+1,s+1}+\lambda m(K)U_K^{n+1,s+1}\\ =&m(K)\left(\lambda U_K^{n+1,s}+f_1(U_K^{n+1,s},V_K^{n+1,s})\right), \end{aligned} \tag{36}$$

$$\begin{aligned} &m(K)\frac{V_K^{n+1,s+1}-V_K^n}{\Delta t}+\sum_{\sigma\in\mathcal{E}_K}\tilde{F}_{K,\sigma}^{n+1,s+1}+\lambda m(K)V_K^{n+1,s+1}\\ =&m(K)\left(\lambda V_K^{n+1,s}+f_2(U_K^{n+1,s+1},V_K^{n+1,s})\right), \end{aligned} \tag{37}$$

for any $K\in\mathcal{J}_{in}$, and subject to $U_K^{n+1,s+1}=g_1(K,t^{n+1})$ and $V_K^{n+1,s+1}=g_2(K,t^{n+1})$ for any $K\in\mathcal{J}_{out}$, $U_K^0=u_0(K)$ and $V_K^0=v_0(K)$ for any $K\in\mathcal{J}_{in}\cup\mathcal{J}_{out}$, where $n\geq 0$, $s\geq 0$. The iterative algorithm is described in Algorithm 1, where we set $\varepsilon=10^{-8}$ in the numerical experiments.

Algorithm 1 The IRP-preserving iteration

```
Compute the initial vector (U^0, V^0);
n = 0;
while t^{n+1} ≤ T do
    Let s = 0;
    Take (U^{n+1,0}, V^{n+1,0}) = (U^n, V^n);
    while ||U^{n+1,s+1} − U^{n+1,s}||_∞ > ε_non or ||V^{n+1,s+1} − V^{n+1,s}||_∞ > ε_non do
        Solve the linear system (36)-(37);
        Let s = s + 1;
    end while
    Let n = n + 1;
end while
```

We prove that the iterative method can preserve the IRP for the coupled quasimonotone parabolic system.

Theorem 4. *Assume that* $\mathbf{f}=(f_1,f_2)$ *is quasimonotone and Lipschitz continuous in* $\Sigma=[m_1,M_1]\times[m_2,M_2]$ *and satisfies* (3)*, the initial and boundary conditions satisfy* $(u_0,v_0)\in\Sigma$, $(g_1,g_2)\in\Sigma$. *Then for any* $\Delta t>0$*, the solution of the iteration* (36)-(37) *satisfies*

$$(U_K^{n,s},V_K^{n,s})\in\Sigma,\quad \forall K\in\mathcal{J},\quad 0\leq n\leq N,\quad s\geq 0. \tag{38}$$

Proof. The proof of this theorem is similar to that of Theorem 1. We assume that the reaction function is mixed quasimonotone, where f_1 is quasimonotone nonincreasing and f_2 is quasimonotone nondecreasing. The proofs for other types of quasimonotone reaction functions are similar. It is easy to see that $(U_K^0,V_K^0)\in\Sigma$ for any $K\in\mathcal{J}_{in}\cup\mathcal{J}_{out}$. Suppose that (38) holds for any $n\leq m+1$, $s\leq s_0$, where $m\geq 0$, $s_0\geq 0$. If (38) is proved for $n=m+1$, $s=s_0+1$, then the theorem follows immediately.

Denote $K_{\max,U}$, $K_{\min,U}$, $K_{\max,V}$, $K_{\min,V}$ such that

$$U_{K_{\max,U}}^{m+1,s_0+1} = \max_{K\in\mathcal{J}} U_K^{m+1,s_0+1}, \quad U_{K_{\min,U}}^{m+1,s_0+1} = \min_{K\in\mathcal{J}} U_K^{m+1,s_0+1},$$
$$V_{K_{\max,V}}^{m+1,s_0+1} = \max_{K\in\mathcal{J}} V_K^{m+1,s_0+1}, \quad V_{K_{\min,V}}^{m+1,s_0+1} = \min_{K\in\mathcal{J}} V_K^{m+1,s_0+1}.$$

The proof can be divided into two steps. The first step is to prove that $U_{K_{\max,U}}^{m+1,s_0+1} \le M_1$.

Let us suppose that $U_{K_{\max,U}}^{m+1,s_0+1} > M_1$ holds. Starting from (36) and using a derivation similar to (23), it follows that

$$\begin{aligned}\frac{U_{K_{\max,U}}^{m+1,s_0+1} - M_1}{\Delta t} \le& \frac{U_{K_{\max,U}}^{m+1,s_0+1} - U_{K_{\max,U}}^{m}}{\Delta t}\\ \le& \lambda(U_{K_{\max,U}}^{m+1,s_0} - U_{K_{\max,U}}^{m+1,s_0+1}) + f_1(U_{K_{\max,U}}^{m+1,s_0}, V_{K_{\max,U}}^{m+1,s_0}).\end{aligned} \tag{39}$$

Since f_1 is nonincreasing with respect to v, we have $f_1(U_{K_{\max,\ U}}^{m+1,s_0},\ V_{K_{\max,\ U}}^{m+1,\ s_0}) \le f_1(U_{K_{\max,\ U}}^{m+1,\ s_0},\ m_2)$. Similar to the derivation of (24), it holds that

$$\begin{aligned}&\frac{U_{K_{\max,U}}^{m+1,s_0+1} - M_1}{\Delta t}\\ &\le \lambda(U_{K_{\max,U}}^{m+1,s_0} - U_{K_{\max,U}}^{m+1,s_0+1}) + f_1(U_{K_{\max,U}}^{m+1,s_0}, m_2) - f_1(M_1, m_2)\\ &\le \lambda(U_{K_{\max,U}}^{m+1,s_0} - M_1) + \lambda(M_1 - U_{K_{\max,U}}^{m+1,s_0})\\ &= 0,\end{aligned} \tag{40}$$

which contradicts $U_{K_{\max,U}}^{m+1,s_0+1} > M_1$. Hence we have $U_{K_{\max,U}}^{m+1,s_0+1} \le M_1$. Similarly, $U_{K_{\min,U}}^{m+1,s_0+1} \ge m_1$ can be proved. It means that $U_K^{m+1,s_0+1} \in [m_1, M_1]$ for any $K \in \mathcal{J}$.

The second step is to show that $V^{m+1,s_0+1} \in [m_2, M_2]$.

If $V^{m+1,s_0+1} \in [m_2, M_2]$ does not hold, then we have $V_{K_{\max,V}}^{m+1,s_0+1} > M_2$ or $V_{K_{\min,V}}^{m+1,s_0+1} < m_2$. Let us suppose that $V_{K_{\max,V}}^{m+1,s_0+1} > M_2$ holds. Similar to (39), it follows that

$$\frac{V_{K_{\max,V}}^{m+1,s_0+1} - M_2}{\Delta t} \le \lambda(V_{K_{\max,V}}^{m+1,s_0} - V_{K_{\max,V}}^{m+1,s_0+1}) + f_2(U_{K_{\max,V}}^{m+1,s_0+1}, V_{K_{\max,V}}^{m+1,s_0}). \tag{41}$$

According to the monotonicity of f_2 with respect to u, we have $f_2(U_{K_{\max,V}}^{m+1,s_0+1}, V_{K_{\max,V}}^{m+1,s_0}) \le f_2(M_1, V_{K_{\max,V}}^{m+1,s_0})$. Similar to the derivation of (40), it can be shown that

$$\frac{V_{K_{\max,V}}^{m+1,s_0+1} - M_2}{\Delta t} \le 0,$$

which contradicts $V_{K_{\max,V}}^{m+1,s_0+1} > M_2$. Hence we have $V_{K_{\max,V}}^{m+1,s_0+1} \le M_2$. Similarly, we can prove that $V_{K_{\min,V}}^{m+1,s_0+1} \ge m_2$. It means that $V_K^{m+1,s_0+1} \in [m_2, M_2]$ for any $K \in \mathcal{J}$. This completes the proof. □

5. Numerical experiments

In this section, numerical examples with different models are presented to demonstrate the accuracy and the IRP-preserving property of the finite volume scheme. Comparison results with the nine-point scheme are provided to illustrate that the

nine-point scheme fails to preserve the invariant regions, indicating the advantage of the IRP-preserving scheme. In the numerical examples, we use

$$\varepsilon_u^2 = \left[\sum_{K\in\mathcal{J}_{in}} \left(U_K - u(K)\right)^2 m(K)\right]^{1/2},$$
$$\varepsilon_v^2 = \left[\sum_{K\in\mathcal{J}_{in}} \left(V_K - v(K)\right)^2 m(K)\right]^{1/2},$$
$$\varepsilon_u^F = \left[\sum_{K\in\mathcal{J}} \left(F_{K,\sigma} - \mathcal{F}_{K,\sigma}\right)^2\right]^{1/2},$$
$$\varepsilon_v^F = \left[\sum_{K\in\mathcal{J}} \left(\tilde{F}_{K,\sigma} - \tilde{\mathcal{F}}_{K,\sigma}\right)^2\right]^{1/2}$$

to evaluate approximate the L^2 errors and the normal flux errors of u and v, respectively.

5.1. Example 1. In the first example, we consider the problem with continuous diffusion coefficients on $\Omega = (0,1)\times(0,1)$. The coefficients $\kappa_1 = R_1 D_1 R_1^{\mathrm{T}}$ and $\kappa_2 = R_2 D_2 R_2^{\mathrm{T}}$, where R_1, R_2, D_1 and D_2 are given by

$$R_1 = \begin{pmatrix} \cos\theta_1 & -\sin\theta_1 \\ \sin\theta_1 & \cos\theta_1 \end{pmatrix}, \quad D_1 = \begin{pmatrix} k_1 & 0 \\ 0 & k_2 \end{pmatrix}$$

and

$$R_2 = \begin{pmatrix} \cos\theta_2 & -\sin\theta_2 \\ \sin\theta_2 & \cos\theta_2 \end{pmatrix}, \quad D_2 = \begin{pmatrix} k_3 & 0 \\ 0 & k_4 \end{pmatrix}.$$

We take $\theta_1 = \frac{5\pi}{12}$, $\theta_2 = \frac{\pi}{3}$, $k_1 = 1 + 2x^2 + y^2$, $k_2 = 1 + x^2 + 2y^2$, $k_3 = 1 + x^2 + 2y^2$, $k_4 = 1 + 2x^2 + y^2$. We set $f_1(u,v) = u(1-u)(u-0.1)$ and $f_2(u,v) = u - v$ and take the exact solution

$$u(x,y,t) = \mathrm{e}^{-t}\sin(\pi x)\sin(\pi y),$$
$$v(x,y,t) = \mathrm{e}^{-t}\cos(\pi x)\cos(\pi y).$$

The exact solution provides the Dirichlet boundary conditions. We add linear source terms in the right sides of the model (1)-(2), which can be calculated from the exact solution correspondingly.

We set the final time $T = 1$ and a sufficiently small time step $\Delta t = 1\text{E-}4$. This example only tests the spatial convergence order, and no investigation on IRP was conducted. Let N_c denote the number of cells. We display the L^2 errors and flux errors on the random quadrilateral and triangular meshes in Tables 2 and 3, respectively. The two types of random meshes are presented in Fig. 2. From these tables, we observe that the L^2 errors achieve a second-order convergence rate on both the random quadrilateral and triangular meshes, and the flux errors achieve a first-order convergence rate on the random quadrilateral meshes and obtain higher than first-order convergence rate on random triangular meshes.

5.2. Example 2. In this example, we test the accuracy of our scheme under the problem with discontinuous diffusion coefficient on $\Omega = (0,1)\times(0,1)$. We consider

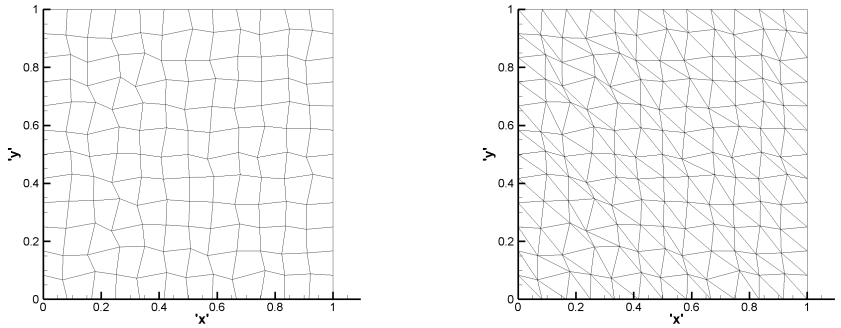

The random quadrilateral meshes. The random triangular meshes.

FIGURE 2. The random meshes.

TABLE 2. The errors for Example 1 on the random quadrilateral meshes.

N_c	144	576	2304	9216
ε_u^2	1.21E-03	3.98E-04	1.04E-04	2.21E-05
order		1.61	1.93	2.23
ε_u^F	1.80E-02	8.27E-03	3.90E-03	2.02E-03
order		1.12	1.08	0.94
ε_v^2	1.60E-03	4.14E-04	1.05E-04	2.63E-05
order		1.94	1.98	1.99
ε_v^F	1.95E-02	8.50E-03	4.00E-03	1.96E-03
order		1.19	1.08	1.02

TABLE 3. The errors for Example 1 on the random triangular meshes.

N_c	288	1152	4608	18432
ε_u^2	9.32E-04	2.45E-04	5.96E-05	1.38E-05
order		1.92	2.03	2.10
ε_u^F	1.98E-02	6.23E-03	2.16E-03	9.31E-04
order		1.66	1.52	1.21
ε_v^2	8.97E-04	2.52E-04	6.31E-05	1.56E-05
order		1.83	1.99	2.01
ε_v^F	1.87E-02	6.65E-03	2.69E-03	1.11E-03
order		1.49	1.30	1.27

the exact solution

$$u(x,y,t)=\begin{cases}\mathrm{e}^{-t}\left(x-\frac{2}{3}\right)\left(x^3+y^3\right), & \text{if } x\le\frac{2}{3},\\ 4\mathrm{e}^{-t}\left(x-\frac{2}{3}\right)\left(x^3+y^3\right), & \text{if } x>\frac{2}{3},\end{cases}$$

$$v(x,y,t)=\begin{cases}\mathrm{e}^{-t}\left(x-\frac{2}{3}\right)\left(x^2-y^2\right), & \text{if } x\le\frac{2}{3},\\ 4\mathrm{e}^{-t}\left(x-\frac{2}{3}\right)\left(x^2-y^2\right), & \text{if } x>\frac{2}{3},\end{cases}$$

and take the diffusion coefficient

$$\kappa_1 = \kappa_2 = \begin{cases} 4I, & \text{if } x \le \frac{2}{3}, \\ I, & \text{if } x > \frac{2}{3}. \end{cases}$$

The functions $f_1(u, v)$ and $f_2(u, v)$ are

$$f_1(u, v) = u^2 - \mathrm{e}^v,$$
$$f_2(u, v) = u^3 - v,$$

and the linear source functions are calculated correspondingly.

We set the final time $T = 1$ and a sufficiently small time step $\Delta t =$ 1E-4 in order to test the spatial accuracy; no investigation of IRP was conducted. Tables 4 and 5 provide the L^2 norm of errors of solutions and fluxes on two types of random meshes. The numerical results reveal that our scheme achieves a second-order convergence rate for the L^2 errors of solutions and a convergence rate higher than first-order for the flux errors.

TABLE 4. The errors for Example 2 on the random quadrilateral meshes.

N_c	144	576	2304	9216
ε_u^2	3.44E-03	8.96E-04	2.26E-04	5.67E-05
order		1.94	1.98	1.99
ε_u^F	2.14E-02	7.63E-03	3.03E-03	1.43E-03
order		1.48	1.33	1.08
ε_v^2	2.26E-03	5.77E-04	1.45E-04	3.66E-05
order		1.96	1.99	1.98
ε_v^F	1.62E-02	5.84E-03	2.38E-03	1.11E-03
order		1.47	1.29	1.10

TABLE 5. The errors for Example 2 on the random triangular meshes.

N_c	288	1152	4608	18432
ε_u^2	2.02E-03	5.44E-04	1.36E-04	3.42E-05
order		1.89	1.99	1.99
ε_u^F	1.41E-02	4.61E-03	1.53E-03	6.10E-04
order		1.61	1.59	1.32
ε_v^2	7.40E-04	2.00E-04	4.94E-05	1.27E-05
order		1.88	2.01	1.95
ε_v^F	1.00E-02	3.24E-03	1.09E-03	4.00E-04
order		1.62	1.56	1.45

5.3. Example 3. In Example 3, we consider a semilinear parabolic system illustrating the superconductivity of liquids, where κ_1 and κ_2 are positive definite diagonal matrices, and the nonlinear reaction-diffusion terms are as follows:

$$f_1(u, v) = (1 - u^2 - v^2)u,$$
$$f_2(u, v) = (1 - u^2 - v^2)v.$$

(f_1, f_2) is quasimonotone nonincreasing in $[0, +\infty) \times [0, +\infty)$. The domain of this example is set to be a square with a hole $\Omega = (0, 1)^2 \backslash [4/9, 5/9]^2$, where internal and external boundaries are denoted by Γ_1 and Γ_2, respectively. Let the diffusion

coefficients κ_1 and κ_2 be discontinuous at Γ, where Γ is composed of four edges of the square $(2/9, 7/9)^2$. The domain Ω is divided into two parts by Γ, where $\Omega_1 = (0,1)^2 \backslash [2/9, 7/9]^2$ and $\Omega_2 = \Omega \backslash \Omega_1$. We take the diffusion coefficients

$$\kappa_1 = \begin{cases} 2I, & \text{in } \Omega_1, \\ \begin{pmatrix} y^2+\varepsilon & -(1-\varepsilon)xy \\ -(1-\varepsilon)xy & x^2+\varepsilon \end{pmatrix}, & \text{in } \Omega_2, \end{cases}$$

$$\kappa_2 = \begin{cases} I, & \text{in } \Omega_1, \\ \begin{pmatrix} y^2+\varepsilon & (1-\varepsilon)xy \\ (1-\varepsilon)xy & x^2+\varepsilon \end{pmatrix}, & \text{in } \Omega_2, \end{cases}$$

where $\varepsilon =$ 5E-3, and take the initial and boundary conditions as

$$g_1(x,y,t) = \begin{cases} 0, & \text{in } \Gamma_1, \\ 1, & \text{in } \Gamma_2, \end{cases} \quad g_2(x,y,t) = \begin{cases} 1, & \text{in } \Gamma_1, \\ 0, & \text{in } \Gamma_2, \end{cases}$$

and

$$u_0(x,y) = \begin{cases} 0, & \text{in } \Omega_1, \\ 1, & \text{in } \Omega_2, \end{cases} \quad v_0(x,y) = \begin{cases} 1, & \text{in } \Omega_1, \\ 0, & \text{in } \Omega_2. \end{cases}$$

It is obvious that $[0,1] \times [0,1]$ is its invariant region, and the Lipschitz constant $\lambda = 5$.

We observe the invariant region properties on random quadrilateral meshes with $N_c = 2916$ and random triangular meshes with $N_c = 5832$, respectively. The numerical solutions are displayed in Figs. 3(A) and 3(B) for random quadrilateral meshes, and in Figs. 3(C) and 3(D) for random triangular meshes, respectively. The minimum and maximum values for U on random quadrilateral meshes are 0 and 1, respectively. Similarly, the minimum and maximum values for V on random triangular meshes are 0 and 1. These numerical results demonstrate the IRPs of our scheme.

TABLE 6. The maxima and minima of the IRP-preserving scheme and nine-point scheme for Example 4 on random quadrilateral meshes.

method	$U_{\max}$	N_c^o	pct	$U_{\min}$	N_c^u	pct
IRP	0	0	0.00%	1	0	0.00%
NP	1.0290	562	15.61%	-2.1341E-02	419	11.64%
	$V_{\max}$	N_c^o	pct	$V_{\min}$	N_c^u	pct
IRP	0	0	0.00%	2	0	0.00%
NP	2.0641	655	18.19%	-4.2454E-02	418	11.61%

5.4. Example 4. In Example 4, we consider a simplified model of the Belousov-Zhabotinski reaction on $\Omega = (0,1) \times (0,1)$, which is a classical model in non-equilibrium thermodynamics. This model takes the reaction functions

$$f_1(u,v) = u(a - bu - cv),$$
$$f_2(u,v) = -uv,$$

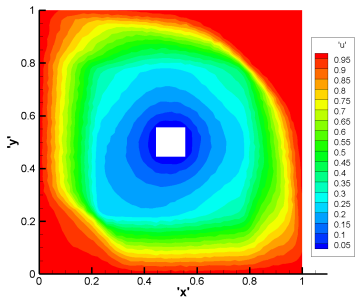

(A) The numerical solution U of the IRP-preserving scheme for Example 3 on the random quadrilateral meshes ($U_{\min} = 0$, $U_{\max} = 1$).

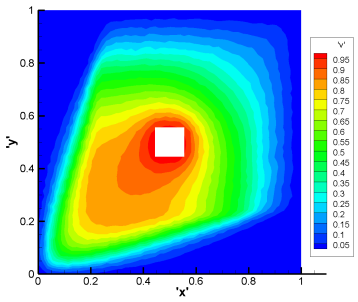

(B) The numerical solution V of the IRP-preserving scheme for Example 3 on the random quadrilateral meshes ($V_{\min} = 1$, $V_{\max} = 1$).

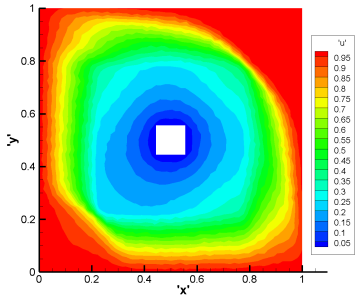

(C) The numerical solution U of the IRP-preserving scheme for Example 3 on the random triangular meshes ($U_{\min} = 0$, $U_{\max} = 1$).

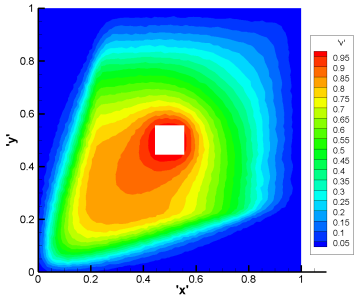

(D) The numerical solution V of the IRP-preserving scheme for Example 3 on the random triangular meshes ($V_{\min} = 0$, $V_{\max} = 1$).

FIGURE 3. The numerical solutions for Example 3.

TABLE 7. The maxima and minima of the IRP-preserving scheme and nine-point scheme for Example 4 on random triangular meshes.

method	$U_{\max}$	N_c^o	pct	$U_{\min}$	N_c^u	pct
IRP	0	0	0.00%	1	0	0.00%
NP	1.0186	699	9.71%	-1.7108E-02	777	10.79%
	$V_{\max}$	N_c^o	pct	$V_{\min}$	N_c^u	pct
IRP	0	0	0.00%	2	0	0.00%
NP	2.0694	1535	21.32%	-4.1207E-02	821	11.40%

where a, b, c are positive constants. When $u \geq 0$ and $v \geq 0$, the functions (f_1, f_2) are quasimonotone nonincreasing, and f_1 and f_2 are Lipschitz continuous in any finite region of (u, v). We set $a = 1$, $b = 2$, $c = 10$ and take the functions

$$u_0(x, y) = g_1(x, y, t) = \begin{cases} 0, & \text{if } 2x - y \leq -\frac{1}{16}, \\ 8(2x - y) + 0.5, & \text{if } -\frac{1}{16} < 2x - y \leq \frac{1}{16}, \\ 1, & \text{if } 2x - y > \frac{1}{16}, \end{cases}$$

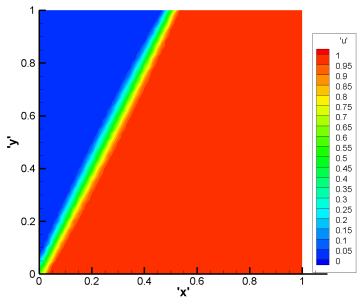

(A) The numerical solution U of the IRP-preserving scheme for Example 4 on the random quadrilateral meshes ($U_{\min} = 0$, $U_{\max} = 1$).

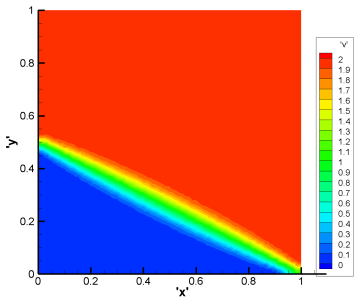

(B) The numerical solution V of the IRP-preserving scheme for Example 4 on the random quadrilateral meshes ($V_{\min} = 0$, $V_{\max} = 2$).

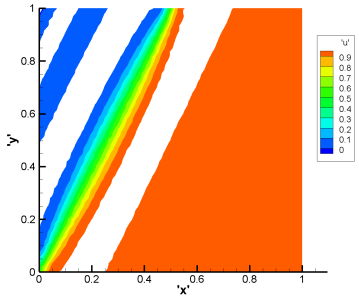

(C) The numerical solution U of the nine-point scheme for Example 4 on the random quadrilateral meshes ($U_{\min} = -2.1341\text{E-}2$, $U_{\max} = 1.0290$).

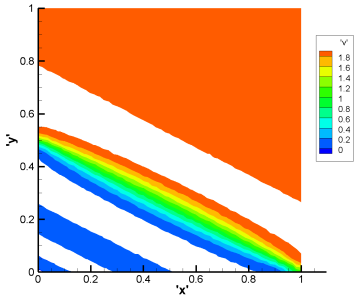

(D) The numerical solution V of the nine-point scheme for Example 4 on the random quadrilateral meshes ($V_{\min} = -4.2454\text{E-}2$, $V_{\max} = 2.0641$).

FIGURE 4. The numerical solutions for Example 4 on quadrilateral meshes.

and

$$v_0(x,y) = g_2(x,y,t) = \begin{cases} 0, & \text{if } x+2y \le \frac{15}{16}, \\ 16(x+2y)-15, & \text{if } \frac{15}{16} < x+2y \le \frac{17}{16}, \\ 2, & \text{if } x+2y > \frac{17}{16}. \end{cases}$$

A simple calculation gives $(u_0, v_0), (g_1, g_2) \in [0,1] \times [0,2]$, the Lipschitz constant $\lambda = 35$. According to Lemma 1, the invariant region of the exact solution is $[0,1] \times [0,2]$.

We set $T = 1$ and $\Delta t = 1\text{E-}3$. We solve the problem using our scheme and the nine-point (N-P) scheme on the random quadrilateral meshes with $N_c = 3600$ and random triangular meshes with $N_c = 7200$, respectively. The numerical solutions are presented in Fig. 4 and Fig. 5. We denote the maximum and minimum of the solution vector U as $U_{\max}$ and $U_{\min}$, respectively. We define $V_{\max}$ and $V_{\min}$ similarly. The numbers of overshoots and undershoots of numerical solution are denoted as N_c^o and N_c^u, and their corresponding percentages are indicated by "pct". Tables 6-7 summarize the maxima and minima, the numbers of overshoots and undershoots,

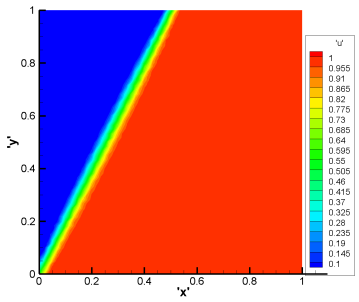

(A) The numerical solution U of the IRP-preserving scheme for Example 4 on the random triangular meshes ($U_{\min} = 0$, $U_{\max} = 1$).

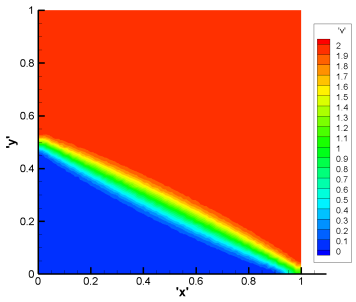

(B) The numerical solution V of the IRP-preserving scheme for Example 4 on the random triangular meshes ($V_{\min} = 0$, $V_{\max} = 2$).

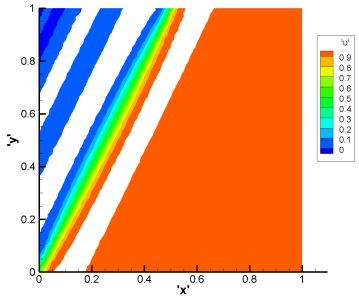

(C) The numerical solution U of the nine-point scheme for Example 4 on the random triangular meshes ($U_{\min} =$ 1.7108E-2, $U_{\max} = 1.0186$).

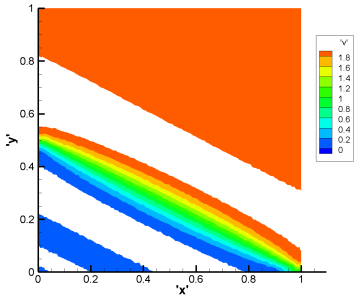

(D) The numerical solution V of the nine-point scheme for Example 4 on the random triangular meshes ($V_{\min} =$ -4.1207E-2, $V_{\max} = 2.0694$).

FIGURE 5. The numerical solutions for Example 4 on triangular meshes.

and their percentages of the two schemes, respectively. As shown in Tables 6-7, the solution of our scheme on both meshes remains within the range of $[0, 1] \times [0, 2]$, whereas the nine-point scheme fails to preserve the IRP. In the latter case, we set the numerical solutions that fall outside the invariant region to white for visual clarity.

6. Conclusion

A finite volume method that preserves the invariant region property is developed for coupled quasimonotone reaction-diffusion systems on general polygonal meshes. The backward Euler method and the DMP-preserving finite volume scheme in [21] are employed to approximate the time derivatives and the diffusion terms, respectively, which yields a nonlinear and conservative scheme. An iterative scheme is constructed to solve the resulting nonlinear system. We prove that both the nonlinear scheme and the iterative method preserve the invariant region property for three types of quasimonotone systems. Finally, numerical examples are provided to illustrate both the accuracy and the IRP-preserving property.

References

[1] Y. Bourgault, Y. Coudire, and C. Pierre, Existence and uniqueness of the solution for the bidomain model used in cardiac electrophysiology, Nonlinear Analysis: Real World Applications, 10 (2009), pp. 458–482.

[2] P. Colli-Franzone, L. Guerri, and B. Taccardi, Modeling ventricular excitation: axial and orthotropic anisotropy effects on wavefronts and potentials, Mathematical Biosciences, 188 (2004), pp. 191–205.

[3] D. Conte, G. Pagano, and B. Paternoster, Nonstandard finite differences numerical methods for a vegetation reactiondiffusion model, Journal of Computational and Applied Mathematics, 419 (2023), p. 114790.

[4] N. Dahmen, J. Droniou, and F. Rogier, A cost-effective nonlinear extremum-preserving finite volume scheme for highly anisotropic diffusion on cartesian grids, with application to radiation belt dynamics, Journal of Computational Physics, 463 (2022), p. 111258.

[5] F. Digne, and J. Michel, Representations of finite groups of Lie type (2nd edn.), Cambridge University Press, 2002.

[6] Q. Du, M. D. Gunzburger, and J. S. Peterson, Analysis and approximation of the Ginzburg-Landau model of superconductivity, SIAM Review, 34 (1992), pp. 54–81.

[7] Q. Du, L. Ju, X. Li, and Z. Qiao, Maximum bound principles for a class of semilinear parabolic equations and exponential time-differencing schemes, SIAM Review, 63 (2021), pp. 317–359.

[8] P. C. Fife, Mathematical aspects of reacting and diffusing systems, Springer-Verlag, 1979.

[9] M. Frittelli, A. Madzvamuse, I. Sgura, and C. Venkataraman, Numerical preservation of velocity induced invariant regions for reactiondiffusion systems on evolving surfaces, Journal of Scientific Computing, 77 (2018), pp. 971–1000.

[10] Y. Gong, B. Ji, and H. Liao, A maximum bound principle preserving iteration technique for a class of semilinear parabolic equations, Applied Numerical Mathematics, 184 (2023), pp. 482–495.

[11] U. Hornung and W. Jger, Diffusion, convection, adsorption, and reaction of chemicals in porous media, Journal of Differential Equations, 92 (1991), pp. 199–225.

[12] J. W. Jerome, Fully discrete stability and invariant rectangular regions for reaction-diffusion systems, SIAM Journal on Numerical Analysis, 21 (1984), pp. 1054–1065.

[13] P. Jiang, J. Ni, and L. Zhu, Global well-posedness and large-time behavior for the equilibrium diffusion model in radiation hydrodynamics, Journal of Function Spaces, (2023), pp. 1–9.

[14] M. Justin, G. Betchewe, S. Y. Doka, and K. T. Crepin, Exact solutions of a semiconductor nonlinear reaction diffusion equation through factorization method, Applied Mathematics and Computation, 219 (2012), pp. 2917–2922.

[15] X. Li, L. Ju, and T.-T.-P. Hoang, Overlapping domain decomposition based exponential time differencing methods for semilinear parabolic equations, BIT Numerical Mathematics, 61 (2021), pp. 1–36.

[16] M. A. Ragusa and F. Wu, Eigenvalue regularity criteria of the three-dimensional mcropolar fluid equations, Bulletin of the Malaysian Mathematical Sciences Society, 47 (2024), pp. 1–11.

[17] J. Sembera and M. Benes, Nonlinear Galerkin method for reactiondiffusion systems admitting invariant regions, Journal of Computational and Applied Mathematics, (2001), pp. 163–176.

[18] Z. Sheng and G. Yuan, A nine point scheme for the approximation of diffusion operators on distorted quadrilateral meshes, SIAM Journal on Scientific Computing, 30 (2008), pp. 1341–1361.

[19] Z. Sheng and G. Yuan, The finite volume scheme preserving extremum principle for diffusion equations on polygonal meshes, Journal of Computational Physics, 230 (2011), pp. 2588–2604.

[20] Z. Sheng and G. Yuan, Construction of nonlinear weighted method for finite volume schemes preserving maximum principle, SIAM Journal on Scientific Computing, 40 (2018), pp. 607–628.

[21] Z. Sheng and G. Yuan, A nonlinear scheme preserving maximum principle for heterogeneous anisotropic diffusion equation, Journal of Computational and Applied Mathematics, 436 (2024), p. 115438.

[22] J. Smoller, Shock waves and reaction-diffusion equations, Springer, 2nd ed., 1999.

[23] R. Spigler and D. H. Zanette, Reaction-diffusion models from the Fokker-Planck formulation of chemical processes, IMA Journal of Applied Mathematics, 49 (1992), pp. 217–229.

[24] J. Tian, Global existence and boundedness of solutions in a reaction-diffusion system of Michaelis-Menten-type predator-prey model with nonlinear prey-taxis and random diffusion, Filomat, 37 (2023), pp. 1535–1547.

[25] H. Zhou, Z. Sheng, and G. Yuan, A finite volume scheme preserving the invariant region property for the coupled system of FitzHugh-Nagumo equations on distorted meshes, Computers & Mathematics with Applications, 117 (2022), pp. 39–52.

School of Mathematics, Jilin University, Changchun, China
E-mail: zhouhuifang@jlu.edu.cn
E-mail: sunyc21@mails.jlu.edu.cn
E-mail: huofc22@mails.jlu.edu.cn